ACS OMEGA

Open Access

http://pubs.acs.org/journal/acsodf

Article

Rheology and Printability of a Porcelain Clay Paste for DIW 3D Printing of Ceramics with Complex Geometric Structures

Yanfang Wu, Junjie Lan, Mingxuan Wu, Wu Zhou, Shaobin Zhou, Hui Yang, Maolin Zhang,* and Yue Li*

Cite This: *ACS Omega* 2024, 9, 26450−26457

Read Online

ACCESS | Metrics & More | Article Recommendations | Supporting Information

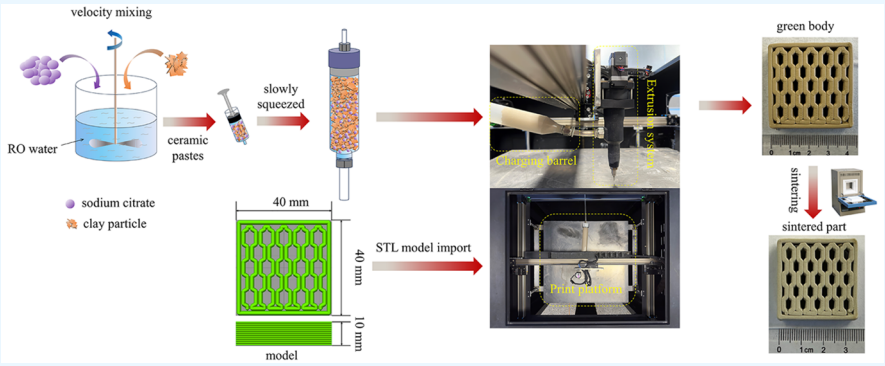

ABSTRACT: The modeling of ceramics with complex geometric structures currently depends on the handcrafted mode, with long cycles, high costs, and low efficiency; additive manufacturing (AM) technology can solve this problem well. Herein, the porcelain clay paste was successfully prepared for the direct ink writing (DIW) 3D printing process of ceramics with complex geometric structures, and the effects of sodium citrate (SC) content on the rheological properties and DIW 3D printability of the porcelain clay paste were investigated in detail. The SC has a vital role in the rheological behavior of porcelain clay paste. Adding SC increases the absolute zeta potential and decreases the viscosity of the paste, while a high SC content will lead to a low storage modulus of the paste. The porcelain clay paste with an SC content of 0.05% and a paste solid content of 75% possesses suitable rheological properties and a storage modulus for DIW 3D printing. The as-prepared porcelain clay paste has high DIW 3D printability at a pressure of 0.5 MPa, and a 3D-printed green body with a well-densified structure can be achieved. After being sintered, the 3D-printed ceramic exhibits high densification and mechanical properties. A green body with complex geometric structures is quickly and precisely modeled by the DIW 3D printing process with the resultant porcelain clay paste as the raw material. This work provides a practical approach to rapidly fabricating ceramics with complex geometrical structures.

1. INTRODUCTION

Molding ceramics with complex geometric structures has always been challenging for ceramic manufacturing. The traditional manufacturing process is time-consuming and expensive for ceramic parts. For example, the modeling of Longquan celadon (a kind of ceramic with a green glaze), containing inorganic components (such as clay minerals, quartz, feldspar, etc.), water, and most commonly modifiers,[1,2] traditionally is in handcraft and molded mode, which lasts for thousands of years.[3] The handcrafted mode allows the product to be unique and adapt to the demands of the customers, but at a high cost and low efficiency. The molded mode has high production efficiency but needs quite a long time for the manufacturing cycle of the initial model.[4] In recent years, additive manufacturing (AM) methods have become increasingly important in the production industry.[5] It is also known as one of the technological breakthroughs revolutionizing product manufacturing, which can be an excellent solution to this problem. Compared with traditional manufacturing technology, the AM methods are applied and developed in ceramic manufacturing due to the high efficiency and irreplaceability to the manufacturing ceramic industry of complex geometric structures.[6]

Several AM methods have been put forward for complex ceramic structure manufacturing, such as selective laser melting/sintering (SLM/SLS),[7] binder jetting,[8] fused deposition modeling of ceramics (FDM/FDC),[9] inkjetting,[10] stereolithography (SLA),[11] and direct ink writing (DIW).[12] DIW is a

Received: March 18, 2024
Revised: May 25, 2024
Accepted: May 29, 2024
Published: June 7, 2024

layer-by-layer 3D printing technique based on the rheology of the paste and the extrusion process. It could flexibly fabricate parts by tuning the moderate rheological behavior of the paste and under proper extrusion pressure through a fine nozzle without auxiliary support structures.[13] Previous studies have shown that the DIW technique allows the printing of practically any material as long as the precursor (such as ink and ceramic paste) can be engineered to demonstrate the appropriate rheological behavior. This DIW technique has emerged as one of the most versatile methods to create complex structures with a wide range of materials.[13−15]

During the DIW 3D printing process, the properties of the precursor (ink, slurry, or paste) are the most crucial for printing performance. For current printing inks, the corresponding printed samples have low molding accuracy, high firing shrinkage, and low strength, limiting the application scope of this technology in the porcelain field.[16,17] However, for the high solid loading paste suitable for manufacturing porcelain, it is a complex and challenging issue to design the porcelain clay paste with an appropriate rheology threshold before printing, avoiding the occurrence of clogs and slumping during printing and retaining its shape after printing.[15] For this issue, some scholars have reported relative findings, such as clay formulation,[15] modifier type and content,[18−21] surface modification,[22−24] printing parameters,[25−28] and solids volume fraction,[29] which are controlled to improve the rheological behavior of the precursor, achieve good printability and physical properties, and prepare high-precision 3D printing samples. Faksawat et al.[30] used 3D printing technology to prepare specific bone production with a bending strength below 40 MPa and a volume shrinkage of about 27% at a sintering temperature of 1200 °C, when 95 wt % clay and 5 wt % hydroxyapatite were selected as raw materials. Revelo et al.[31] prepared the 3D-printed samples with an optimized compressive strength of 38 MPa at the sintering temperature of 1100 °C, when 63.7 wt % kaolinite and 36.3 wt % water were used as raw materials. Among these, the surface modifier is one of the most effective methods for reaching the moderate rheology threshold suitable for 3D printing. Dispersant Disperbyk-180 for steric stabilization,[18] Dispex A40 for zeta potential and pH regulation,[19] Disperbyk (BYK, copolymer with acidic groups) as a wetting and dispersing agent,[20] and sodium citrate[32,33] and the like were employed to optimize the rheological behavior of the precursor and the suitability for DIW 3D printing. Among these, sodium citrate (SC) is one of the most widely used rheological regulators and retarders in many fields. Ramachandran et al.[32] and Rottstegge et al.[33] found that cement paste had good hydration retardation due to the presence of SC so that the fresh cement slurry can maintain plasticity for a more extended period. Thus, these modifiers were often selected to regulate the rheological behavior, targeting different precursor properties to obtain a viscoelastic paste with sufficient stiffness and stability for printing. Furthermore, different from other modifiers, SC is a nontoxic viscosity-modifying additive, which has pH regulatory function and good chelating ability to metal ions such as Ca^{2+}, Mg^{2+}, and Fe^{3+} (similar to the main chemical compositions of porcelain clay materials), playing an essential role in retarding and stabilizing.[33] Additionally, limited studies have explored the rheological characteristics of high-solid-loading porcelain clay paste incorporating various concentrations of sodium citrate and subsequently employing the clay paste in intricate geometric constructions through DIW 3D printing.

In this work, SC was chosen as a rheology regulator, and the influence of sodium citrate dihydrate content on the rheology and printability of high-solid-loading porcelain clay paste via DIW 3D printing was investigated. Specifically, Longquan Diyao clay was utilized as the primary raw material, with sodium citrate dihydrate serving as the dispersant, and a mixing process was employed to prepare the modified paste samples. The effect of varying SC content in the aqueous clay paste on its rheological properties and printability via DIW has been studied. The influence of SC content on the zeta potential, pH, rheological behavior, and printing parameters was evaluated. By adjusting the amount of SC and the extruded pressure, the clogs and printable and slumping regions of DIW 3D printing were provided, and a printability diagram was proposed. Also, the mechanical properties of the sintered sample were evaluated. This study provides a novel DIW 3D printing method for the preparation of Longquan celadon using high-solid-loading ceramic paste containing a controlled modifier content.

2. MATERIALS AND METHODS

2.1. Preparation of Porcelain Clay Paste. A commercially available Longquan Diyao clay for the ceramic paste was purchased from Zhejiang Tianfeng Ceramics Co., Ltd. The SC (purity 99.0%, $C_6H_5Na_3O_7{\cdot}2H_2O$), which was the modifier component used as a rheology regulator for the ceramic paste, was purchased from Shanghai Aladdin Biochemical Technology Co., Ltd.

The solid content directly affects the physical properties of the paste directly. Typically, ceramic slurry with a solid content of 75% is commonly used in manufacturing processes due to its favorable physical properties, allowing it to maintain shape effectively.[34] Five different mass fractions (0, 0.025, 0.05, 0.075, and 0.1 wt %) of SC were added to the reverse osmosis (RO) water (the mass fraction of RO water was 25 wt %). Subsequently, a high-speed mixer (GJ-3S, Hengtaida, Qingdao) was utilized to stir the mixture for 5 min. Following this, 75 wt % mass fractions of clay were gradually added to the mixture while stirring at a speed of 300 rpm for 30 min. Consequently, modified pastes with varying SC contents were prepared and designated as S-0, S-1, S-2, S-3, and S-4. The pastes were loaded into 100 mL plastic disposable syringe barrels, followed by a piston at the larger opening of the barrel (see Figure S2). The paste was slowly squeezed into the 3D printed bin to avoid air entry and then installed in the printer.

2.2. DIW 3D Printing of Porcelain Clay Paste. A square model was designed as a structure with a log-pile lattice in this experiment to evaluate the printable performance of the pastes. A sample with more complex geometric structures (e.g., the logo of Zhejiang University) was prepared by layers of parallel printed lines. The green bodies were prepared by the DIW technique using a self-developed DIW 3D printing device (D5050, Zhejiang University, China). After drying and sintering, a series of sintered ceramic parts could be fabricated (Figure S3). The DIW 3D printing parameters were as follows: the pneumatic pressure was 0.1−0.6 MPa. The diameter of the printing needle was fixed to 1.6 mm, the layer height was 0.8 mm, and the printing speed was 50 mm/s.

2.3. Drying and Sintering Process of the DIW 3D-Printed Green Body. The drying and sintering processes of the DIW 3D-printed green bodies were demonstrated in detail. The printed green bodies were covered with a ripped plastic wrap for 24 h to keep the shape steady and then exposed to air

https://doi.org/10.1021/acsomega.4c02543
ACS Omega 2024, 9, 26450−26457

drying for 48 h. Then, the samples were sintered in air at atmospheric pressure in a furnace (KSL-1750X, Kejing, China). The temperature ramps were 5 °C/min from room temperature to 480 °C during the heating process, and the holding temperature was maintained at 480 °C for 0.5 h. Then, the temperature ramps were both 8 °C/min during the heating process from 480 to 980 °C, and the holding temperature was maintained at 980 °C for 1 h. 3 °C/min was used during the heating process from 980 °C up to 1280 °C, and the holding temperature was maintained at firing temperatures for 20 min. Subsequently, the samples were slowly cooled to room temperature in the furnace. Eventually, a series of fired 3D-printed ceramics were fabricated.

2.4. Characterization. Zeta potential and pH measurements of the modified pastes were carried out using a Malvern Zetasizer (Malvern, Zetasizer Ultra, U.K.) and a pH meter (Leici, PHS-3, China), and its detailed testing process is shown in the Supporting Information. The rheological properties of the pastes were characterized by a stress-controlled rheometer (HAAKE, MARS 60, Germany). The diameter and the plate−plate gap were 25 mm and 0.15 mm, respectively. The temperature was 25 °C. The rheological properties of all of the pastes were characterized from 0.01 to 1000 s^{-1}. Thixotropic characteristics of the current pastes were estimated with shear rates from 0 to 500 s^{-1}. Finally, the viscoelastic response was measured by an oscillation method from the linear viscoelastic region, in which the storage modulus (G') and loss modulus (G'') were obtained at shear stress values from 0.01 to 1000 Pa at a frequency of 1 Hz. The bending strength was measured by a strength tester (INSTRON, INSTRON3366, U.K.), and its detailed testing process is shown in the Supporting Information.

An image size measuring instrument (IM-8020, KEYENCE, Japan) was employed to capture high-precision projection images and measure the dimensions of the specified position.

3. RESULTS AND DISCUSSION

3.1. Rheological Behavior of Porcelain Clay Pastes. Rheological behaviors of porcelain clay pastes are listed in Figure 1. Figure 1a shows the relationship between the viscosity and shear rate. It indicates shear-thinning behavior at a shear rate of 0−85 s^{-1} for all pastes. The fluidity of the paste was lower in the low shear rate region, thereby facilitating mechanical support for the 3D-printing components and preventing structural collapse. The paste was fluid in the high region, and its viscosity decreased as the rate of shear increased, which was beneficial for paving the pastes on the printing platform.[35] Thus, the viscosities decrease with the increase in shear rates, corresponding to the typical rheological behavior of a non-Newtonian fluid.[36,37] Compared to S-0, samples S-1 to S-3 showed a slow decline in the viscosity of the pastes. A distant shear plateau could be observed as the shear rate increased from 20 to 85 s^{-1}, which was beneficial to the steady reprinting of stable thin layers to fabricate the green body with a few defects between adjacent layers.[34,38] However, S-4 showed sharply decreased viscosity (<10 Pa·s at 20−85 s^{-1}) of the paste because of the high concentration of SC, resulting in an extensive degree of shear-thinning behavior that hampers effective formation.

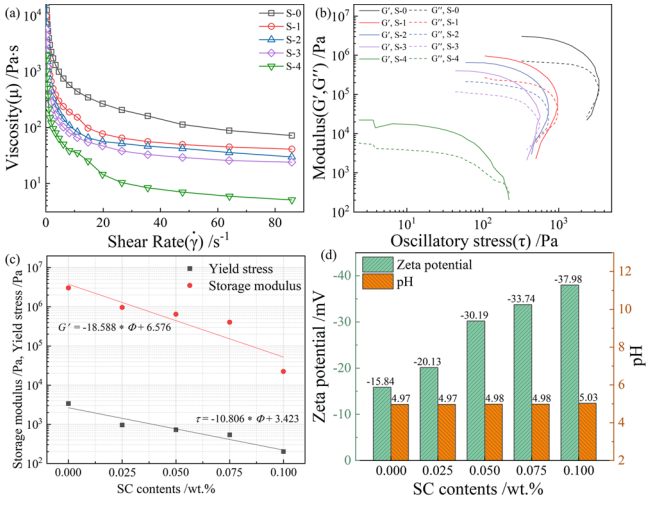

Figure 1. Viscosity (a), storage modulus (b), and zeta potential and pH (d) of the porcelain clay paste with different SC contents and fitting curves for the storage modulus and yield stress vs SC content (c).

Figure 1b shows the storage modulus (G') and loss modulus (G'') curves for the pastes. The G' values were higher than the G'' values for all pastes. With increasing τ, the G' and G'' of all pastes decreased rapidly, which explains the shear-thinning behavior of the paste.[29] As the SC content increases, initial G' and G'' values declined gradually. Notably, the G' and G'' of S-4 are the lowest among all pastes, indicating rapid initiation of viscous flow even at minimal oscillatory stress. Thus, in this case, the moderate rheology threshold achieved by adjusting SC content is as follows: viscosity (μ) around 10^2 Pa·s, oscillatory stress (τ) = 10^2−10^3, and storage modulus (G') = 10^5−10^6 Pa. These findings were comparable to those reported by other researchers utilizing the DIW-3D technique.[39−42]

The storage modulus and yield stress curves are listed in Figure 1c. It can be found that the storage modulus and yield stress decreased linearly as the SC content increased; the corresponding linear relationships are as follows

$$G' = -18.588\Phi + 6.576 \quad (1)$$

$$\tau = -10.806\Phi + 3.423 \quad (2)$$

where G' is the storage modulus, τ is the yield stress, and Φ is the SC content.

Figure 1d displays the zeta potential (ζ) and pH of the pastes. With the SC content increased, the absolute zeta potential ($|\zeta|$) presented an increasing trend while the pH value changed very little. It is worth mentioning that a slight increase in pH is probably due to the hydrolyzed ions of SC being adsorbed on negatively charged clay particles, resulting in the change of the paste.[40] This also increased the value of the absolute zeta potential $|\zeta|$. There is a noticeable increase in the absolute zeta potential $|\zeta|$ from 15.84 up to 37.98 mV within a moderate acidity pH range (4.97 to 5.03).

Based on the analysis of the above results, an appropriate amount of dispersant SC can effectively regulate the rheological properties of the clay paste, including the viscosity and modulus. Herein, a possible mechanism diagram outlining the rheological regulation behavior of clay paste based on the dilution effect of SC dispersants is proposed and presented in Figure 2. The SC dispersant is characterized as a viscosity-modifying additive. The carboxylate groups attach to the surface of the clay particles by ionic binding and then increase the surface charge. This process enhances the electrostatic repulsion between clay particles, prevents particle aggregation,

https://doi.org/10.1021/acsomega.4c02543
ACS Omega 2024, 9, 26450−26457

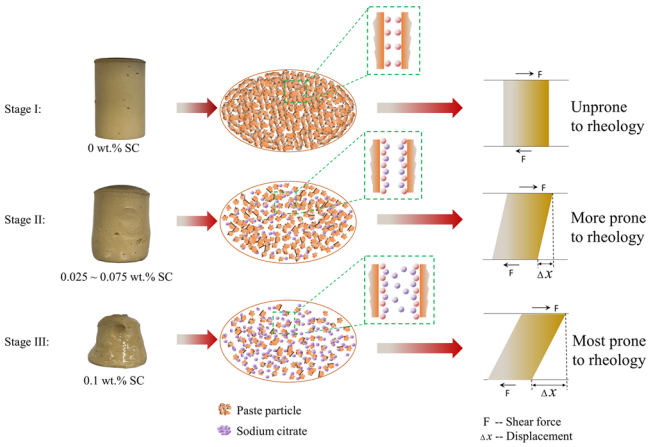

Figure 2. Mechanism diagram of the rheological behavior of the porcelain clay pastes with different SC contents.

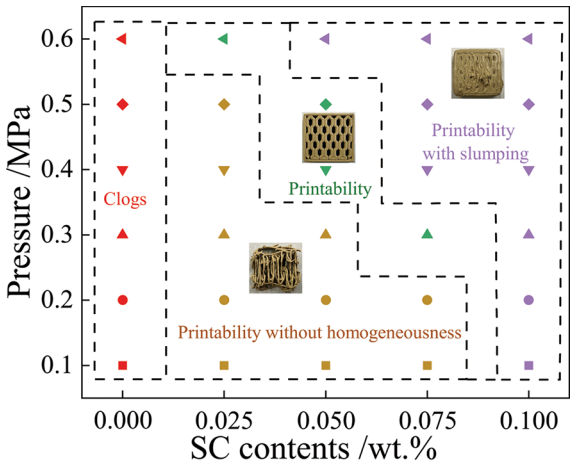

Figure 3. Printability diagram of clogging, printable, and slumping regions for porcelain clay pastes with different SC contents and extrusion pressure.

and ultimately improves the dispersity and rheological properties of the system.[43−45] Without SC, the paste particles were distributed discretely between each other with the sample S-0 exhibiting the lowest zeta potential, G' and G'', rendering the paste less susceptible to rheological changes under external force and increasing the difficulty of extrusion molding at stage I. However, with an increase in SC content from 0.025 to 0.075 wt %, the adsorption capacity on the surface of clay particles increased, resulting in an increase in $|\zeta|$ value and a downward trend in G' and G'' at stage II. Consequently, the paste becomes more responsive to rheological changes under external force, reducing the difficulty of extrusion molding. Nevertheless, when the SC content exceeds 0.1 wt %, the adsorption capacity on the particle surface may saturate, leading to excess and free dispersant molecules bridging between the particles, causing flocculation and reducing the dispersion uniformity of the paste, at stage III. Consequently, the paste exhibits heightened rheological behavior under external forces, facilitating extrusion but challenging the maintenance of shape.[46]

3.2. DIW 3D Printability of Porcelain Clay Pastes. Effective optimization of paste rheology and formulation is critical to ensuring printability and achieving the fabrication of self-supporting ceramic structures with precise dimensional accuracy.[47]

The as-prepared pastes underwent the DIW printing technique to evaluate their shape retention and self-supporting capability. Figure 3 shows the printability diagram relating SC content and pressure to clogging, printable, and slumping regions. Clogging occurred with the 0 wt % SC paste, rendering it unable to be extruded even at maximum printer pressure. When the SC content was 0.025 wt %, the paste could be extruded slowly under pressure ranging from 0.1 to 0.5 MPa but lacked the ability to support model printing. However, model printing became feasible with a pressure increase to 0.6 MPa. When the SC content increased to 0.05 wt %, the paste exhibited better printability at pressures of 0.4 and 0.5 MPa.

Nevertheless, the paste flowed easily by turning the pressure to 0.6 MPa, resulting in consistent slumping occurrences. When the SC content was 0.075 wt %, the paste could be printed at a pressure of 0.3 MPa, but any further increase in SC content led to an inability to maintain the model's shape. With the SC content reaching 0.1 wt %, the paste was extruded effortlessly, but all models failed to retain their shape, even at a pressure of as low as 0.1 MPa, mainly due to the low viscosity and storage modulus. Notably, pastes containing 0.05 wt % SC exhibited successful extrusion and maintained their shape after printing at pressures of 0.4 and 0.5 MPa, while those with 0.025 wt % SC could sustain their shape at 0.6 MPa pressure and those with 0.075 wt % SC, at 0.3 MPa pressure. This observation aligns with the earlier proposition that the pastes can achieve three-dimensional structures with excellent shape retention within an appropriate range of rheology thresholds.

3.3. Microstructures and Properties of DIW 3D-Printed Green Bodies and Sintered Bodies. Dimensional accuracy and microstructure are crucial criteria for evaluating the quality of 3D-printed green bodies.[35,48] To investigate the influence of varying dispersant content and extrusion pressure on the dimensional accuracy of the printed samples, a model size of 40 × 40 × 10 mm^3 was selected. Following a 5 h drying period, various characterizations were carried out on the printed green bodies.

The green body, printed with 0.025 wt % SC-modified paste, was the first in a systematic series of experiments. It demonstrated a viscosity at a shear plateau of about 44.93 Pa·s at the extruded pressure of 0.6 MPa and was named S-1 (see Figure 4a_1,a_2). This was followed by the 0.05 wt % SC-modified paste, with a viscosity at a shear plateau of about 35.78 Pa·s at extruded pressures of 0.4 and 0.5 MPa, named S-2a (see Figure 4b_1,b_2) and S-2b (see Figure 4c_1,c_2). Finally, the 0.075 wt % SC-modified paste, with a viscosity at a shear plateau of about 25.76 Pa·s at the extruded pressure of 0.3 MPa, was named S-3 (see Figure 4d_1,d_2).

To evaluate dimensional accuracy, measurements of the layer width, total width, layer thickness, and total thickness were proposed (Table 1). Some interstices (white arrow) were observed in S-1 and some excess materials (white arrow) were observed in S-3, but no similar phenomena were observed in S-2a and S-2 b. Furthermore, S-2a and S-2b had similar layer thicknesses, while, by comparison of the measured layer width marked in the figure, S-2a had a slightly larger fluctuation than that of S-2b. By comparing these dimensions and appearance, it is evident that the closest match to the model of the sample was achieved with 0.05 wt % SC content and an extrusion pressure of 0.5 MPa.

https://doi.org/10.1021/acsomega.4c02543
ACS Omega 2024, 9, 26450−26457

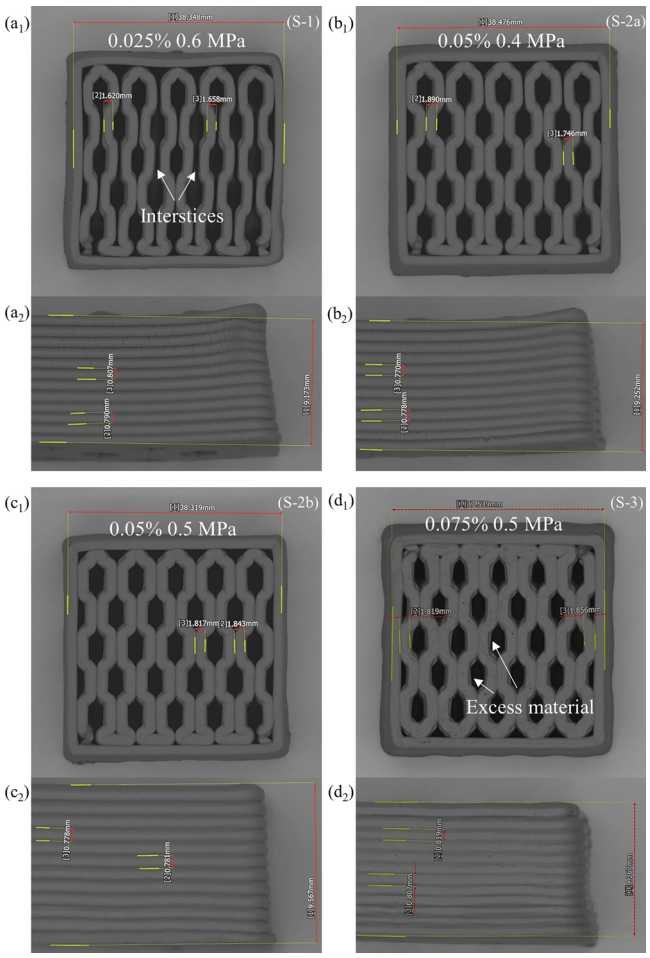

Figure 4. Dimensional accuracy of DIW 3D-printed green body samples with different SC contents and pressures: (a_1, a_2) 0.025 wt % SC content, extrusion pressure 0.6 MPa; (b_1, b_2) 0.05 wt % SC content, extrusion pressure 0.4 MPa; (c_1, c_2) 0.025 wt % SC content, extrusion pressure 0.5 MPa; and (d_1, d_2) 0.075 wt % SC content, extrusion pressure 0.3 MPa.

Table 1. Properties of the DIW 3D-Printed Ceramic Samples Sintered at 1280 °C

Properties	S-1	S-2a	S-2b	S-3
Extrusion pressure/MPa	0.6	0.4	0.5	0.3
SC content/wt %	0. 025	0.05	0.05	0.075
Average layer width/mm	1.639	1.818	1.830	1.838
Total width/mm	38.348	38.476	38.319	37.539
Average layer thickness/mm	0.799	0.774	0.779	0.813
Total thickness/mm	9.173	9.252	9.567	9.367
Bending strength/MPa	50.73	52.13	57.44	58.90
Volume density/g/cm^3	2.2605	2.2649	2.2943	2.3026
Water absorption/%	0.23	0.21	0.11	0.09
Shrinkage/% length (X)	13.78	13.08	12.72	11.65
Width (Y)	14.58	14.47	13.98	13.07
Height (Z)	21.26	20.84	19.73	18.89

Figure 5 shows the fracture morphologies of typical 3D-printed green bodies sintered at 1280 °C. S-1 and S-2a present many voids in the fracture surface (Figure 5a and Figure 5b). When the extruded pressure increased to 0.5 MPa, S-2b showed the disappearance of square cavities, leaving behind some small sintered voids (see Figure 5c). This suggests that

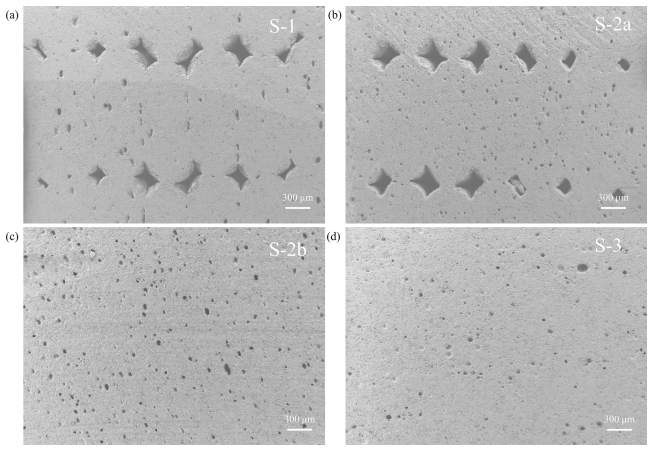

Figure 5. Fracture morphologies of DIW 3D-printed green bodies with different SC contents and pressures: (a) 0.025 wt % SC content, extrusion pressure 0.6 MPa; (b) 0.05 wt % SC content, extrusion pressure 0.4 MPa; (c) 0.025 wt % SC content, extrusion pressure 0.5 MPa; and (d) 0.075 wt % SC content, extrusion pressure 0.3 MPa.

higher pressure can enhance the interaction between layers at the same viscosity of the paste, promoting a densification process. Conversely, with an increase in SC content up to 0.075 wt % at a pressure of 0.3 MPa, the morphology of S-3 showed fewer voids compared to S-2b (see Figure 5d). This is likely due to the lower viscosity of the paste that can readily initiate flow, leading to a reduction in void creation. These fracture morphologies explain the shrinkage change trend observed in the corresponding sample.

The DIW 3D-printed samples were sintered at 1280 °C to evaluate the physical properties of the samples. The experiments were repeated four times for each group. As shown in Table 1, an increase in SC content corresponded to an upward trend in bending strength, volume density, and shrinkage of the sintered samples, while their water absorption presented a downward trend from 0.23 to 0.09%. Specifically, at 0.025 wt % SC content and an extrusion pressure of 0.6 MPa, S-1 exhibited an average bending strength of 50.73 MPa and a volume density of 2.2605 g/cm^3, with a shrinkage for length, width, and height at 13.78, 14.58, and 21.26%, respectively. Upon increasing the SC content up to 0.05 wt %, the average bending strength and volume density increased. At an extrusion pressure of 0.4 MPa, S-2a demonstrated a bending strength of 52.13 MPa and a volume density of 2.2649 g/cm^3, with shrinkages in length, width, and height of 13.08, 14.47, and 20.84%, respectively. Conversely, at an extrusion pressure of 0.5 MPa, S-2b exhibited a bending strength of 57.44 MPa and a volume density of 2.2943 g/cm^3, with shrinkage values at 12.72, 13.98, and 19.73%. Further increase in the SC content to 0.075 wt % led to S-3 achieving an average bending strength and volume density of 58.9 MPa and 2.3026 g/cm^3, with reduced shrinkage in all three directions to 11.65, 13.07, and 18.89%, respectively. S-3 demonstrated optimal bending strength and volume density due to the lower viscosity of the pastes resulting from increased SC content, thereby yielding a higher volume density in the sintered samples.

3.4. DIW 3D Printing Application in Complex Geometric Ceramics. After optimizing the rheology and printability of SC-modified paste, a complex geometric 3D-printed sample of the Zhejiang University school badge was successfully prepared (see Figure 6). All samples utilized the

https://doi.org/10.1021/acsomega.4c02543
ACS Omega 2024, 9, 26450−26457

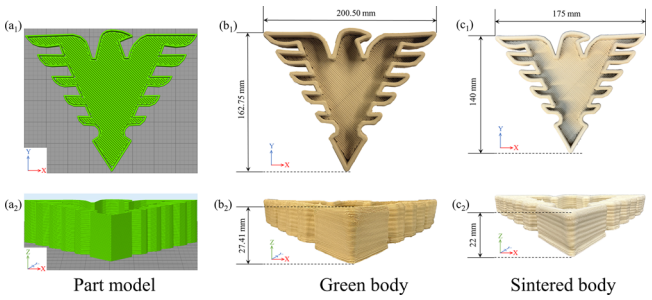

Figure 6. DIW-3D-printed part model (a_1, a_2), green body (b_1, b_2), and its sintered body (c_1, c_2) by using the ceramic paste containing 0.05 wt % SC dispersant.

optimal clay paste formulation through DIW 3D printing, followed by sintering at 1280 °C. As shown in Table 2, the

Table 2. Properties Comparison of DIW 3D Printing and Traditional Handcrafted Mode for Complex Geometric Ceramics Production

Properties	DIW 3D printing mode	Handcrafted mode
Manufacturing cycle	10 min	15 days
Continuous working time	24 h	4 h
Bending strength/MPa	55−60	50−60

bending strength of DIW 3D-printed samples was comparable to that of the samples produced by traditional handcrafted methods. DIW 3D printing shows significant advantages in terms of the manufacturing cycle and continuous working time compared with traditional handcrafted methods. Hence, this study references DIW 3D-printed ceramic parts with high solid loading ceramic paste containing the proper modifier content, which can be applied to complex geometric ceramic production, and the proposed approach can achieve a higher strength than other clay-based 3D printing.[30,31]

4. CONCLUSIONS

A porcelain clay paste with a controllable rheology behavior and storage modulus was prepared for DIW 3D printing of green bodies. The addition of SC as the dispersant affected the rheological behavior of porcelain clay paste. With increasing SC content, the paste exhibited an increase in absolute zeta potential and a slow decline in viscosity, with Newtonian fluid behavior observed at a shear rate of 20 to 85 s^{-1}. Specifically, the porcelain clay paste has an absolute zeta potential of 30.19−33.74 mV, a viscosity of around 10^2 Pa·s, an oscillatory stress of 10^2−10^3, and a storage modulus of 10^5−10^6 Pa, rendering it suitable for DIW 3D printing with superior printability. When the SC content is 0.05 wt % and the pressure of DIW 3D printing is 0.5 MPa, the printed green body sample exhibited optimal dimensional accuracy while the sintered body sample displayed a bending strength of 57.44 MPa. Complex geometric ceramics were fabricated using the DIW-3D printing process with the formulated porcelain clay pastes as the raw material, showing similar physical properties compared to those made by the traditional handcrafted technique.

ASSOCIATED CONTENT

Supporting Information

The Supporting Information is available free of charge at https://pubs.acs.org/doi/10.1021/acsomega.4c02543.

Phase composition, particle size distribution, and morphologies of the clay; fabrication process of the high-solid-loading pastes; preparation process of the DIW-3D-printed green bodies and its sintered parts; and printability diagram of clogs and printable and slumping regions for porcelain clay pastes with different SC contents and extrusion pressures (PDF)

AUTHOR INFORMATION

Corresponding Authors

Maolin Zhang − *Research Center of Ancient Ceramic, Jingdezhen Ceramic University, Jingdezhen 333001, China*; Email: zhangmaolin@jcu.edu.cn

Yue Li − *School of Materials Science and Engineering, Zhejiang University, Hangzhou 310058, China; Institute of Wenzhou, Zhejiang University, Wenzhou 325006, China*; Email: liyue8@zju.edu.cn

Authors

Yanfang Wu − *School of Materials Science and Engineering, Zhejiang University, Hangzhou 310058, China; Key Laboratory of Traditional Heated-Form Craft Technology and Digital Design, China Academy of Art, Hangzhou 310024, China*

Junjie Lan − *Institute of Wenzhou, Zhejiang University, Wenzhou 325006, China*; orcid.org/0000-0002-2177-4799

Mingxuan Wu − *Chinese Celadon Institute, Lishui University, Lishui 323000, China*

Wu Zhou − *Key Laboratory of Traditional Heated-Form Craft Technology and Digital Design, China Academy of Art, Hangzhou 310024, China*

Shaobin Zhou − *Key Laboratory of Traditional Heated-Form Craft Technology and Digital Design, China Academy of Art, Hangzhou 310024, China*

Hui Yang − *School of Materials Science and Engineering, Zhejiang University, Hangzhou 310058, China; Institute of Wenzhou, Zhejiang University, Wenzhou 325006, China*

Complete contact information is available at: https://pubs.acs.org/10.1021/acsomega.4c02543

Notes

The authors declare no competing financial interest.

ACKNOWLEDGMENTS

The authors acknowledge the Key Laboratory of Traditional Heated-Form Craft Technology and Digital Design (China Academy of Art), Ministry of Culture and Tourism for research funding (grant number: TK2021123101).

REFERENCES

(1) Stempkowska, A.; Mastalska-Popławska, J.; Izak, P.; Ogłaza, L.; Turkowska, M. Stabilization of Kaolin Clay Slurry with Sodium Silicate of Different Silicate Moduli. *Appl. Clay Sci.* **2017**, *146*, 147−151.

(2) M'Barki, A.; Bocquet, L.; Stevenson, A. Linking Rheology and Printability for Dense and Strong Ceramics by Direct Ink Writing. *Sci. Rep.* **2017**, *7* (1), 6017.

(3) Zhang, B.; Zhang, M.; Li, Y.; Cheng, H.; Zheng, J. PIXE Study on Recovery of Making-Technology of Chinese Longquan Celadon Made in the Southern Song Dynasty (1127−1279 CE). *Ceram. Int.* **2019**, *45* (3), 3081−3087.
(4) Castro E Costa, E.; Duarte, J. P.; Bártolo, P. A Review of Additive Manufacturing for Ceramic Production. *Rapid Prototyping J.* **2017**, *23* (5), 954−963.
(5) Ali, Md. H.; Batai, S.; Sarbassov, D. 3D Printing: A Critical Review of Current Development and Future Prospects. *Rapid Prototyping J.* **2019**, *25* (6), 1108−1126.
(6) Romanczuk-Ruszuk, E.; Sztorch, B.; Pakuła, D.; Gabriel, E.; Nowak, K.; Przekop, R. E. 3D Printing Ceramics—Materials for Direct Extrusion Process. *Ceramics* **2023**, *6* (1), 364−385.
(7) Ur Rehman, A.; Saleem, M. A.; Liu, T.; Zhang, K.; Pitir, F.; Salamci, M. U. Influence of Silicon Carbide on Direct Powder Bed Selective Laser Process (Sintering/Melting) of Alumina. *Materials* **2022**, *15* (2), 637.
(8) Grant, L. O.; Higgs, C. F.; Cordero, Z. C. Sintering Mechanics of Binder Jet 3D Printed Ceramics Treated with a Reactive Binder. *J. Eur. Ceram. Soc.* **2023**, *43* (6), 2601−2613.
(9) Smirnov, A.; Seleznev, A.; Peretyagin, P.; Bentseva, E.; Pristinskiy, Y.; Kuznetsova, E.; Grigoriev, S. Rheological Characterization and Printability of Polylactide (PLA)-Alumina (Al_2O_3) Filaments for Fused Deposition Modeling (FDM). *Materials* **2022**, *15* (23), 8399.
(10) Bagishev, A. S.; Mal'bakhova, I. M.; Vorob'ev, A. M.; Borisenko, T. A.; Asmed'yanova, A. D.; Titkov, A. I.; Nemudryi, A. P. Layer-by-Layer Formation of the NiO/CGO Composite Anode for SOFC by 3D Inkjet Printing Combined with Laser Treatment. *Russ J. Electrochem* **2022**, *58* (7), 600−605.
(11) Chen, J.; Su, R.; Zhai, X.; Wang, Y.; Gao, X.; Zhang, X.; Zhang, Y.; Zhang, Y.; Liu, S.; He, R. Improving the Accuracy of Stereolithography 3D Printed Al_2O_3 Microcomponents by Adding Photoabsorber: Fundamentals and Experiments. *J. Mater. Res. Technol.* **2023**, *27*, 757−766.
(12) Zhao, Y.; Zhu, J.; He, W.; Liu, Y.; Sang, X.; Liu, R. 3D Printing of Unsupported Multi-Scale and Large-Span Ceramic via near-Infrared Assisted Direct Ink Writing. *Nat. Commun.* **2023**, *14* (1), 2381.
(13) Saadi, M. A. S. R.; Maguire, A.; Pottackal, N. T.; Thakur, M. S. H.; Ikram, M. Md.; Hart, A. J.; Ajayan, P. M.; Rahman, M. M. Direct Ink Writing: A 3D Printing Technology for Diverse Materials. *Adv. Mater.* **2022**, *34* (28), 2108855.
(14) Revelo, C. F.; Colorado, H. A. 3D Printing of Kaolinite Clay Ceramics Using the Direct Ink Writing (DIW) Technique. *Ceram. Int.* **2018**, *44* (5), 5673−5682.
(15) Ordoñez, E.; Gallego, J. M.; Colorado, H. A. 3D Printing via the Direct Ink Writing Technique of Ceramic Pastes from Typical Formulations Used in Traditional Ceramics Industry. *Appl. Clay Sci.* **2019**, *182*, 105285.
(16) Chen, Z.; Li, J.; Liu, C.; Liu, Y.; Zhu, J.; Lao, C. Preparation of High Solid Loading and Low Viscosity Ceramic Slurries for Photopolymerization-Based 3D Printing. *Ceram. Int.* **2019**, *45* (9), 11549−11557.
(17) Tong, W.; Jaw, W. Q.; Pothunuri, L.; Soh, E.; Ferrand, H. L. Easily Applicable Protocol to Formulate Inks for Extrusion-Based 3D Printing. *Cerâmica* **2022**, *68* (386), 152−159.
(18) Hossain, S. S.; Son, H.-J.; Park, S.; Bae, C.-J. Extrusion-Based 3D Printing Alumina-Silica Inks: Adjusting Rheology and Sinterability Incorporating Waste Derived Nanoparticles. *J. Eur. Ceram. Soc.* **2023**, *43* (11), 4865−4876.
(19) Nan, B.; Olhero, S.; Pinho, R.; Vilarinho, P. M.; Button, T. W.; Ferreira, J. M. F. Direct Ink Writing of Macroporous Lead-free Piezoelectric $Ba_{0.85}Ca_{0.15}Zr_{0.1}Ti_{0.9}O_3$. *J. Am. Ceram. Soc.* **2019**, *102* (6), 3191−3203.
(20) Sun, J.; Binner, J.; Bai, J. Effect of Surface Treatment on the Dispersion of Nano Zirconia Particles in Non-Aqueous Suspensions for Stereolithography. *J. Eur. Ceram. Soc.* **2019**, *39* (4), 1660−1667.
(21) Sun, Q.; Yang, Z.; Cheng, H.; Peng, Y.; Huang, Y.; Chen, M. Creation of three-dimensional structures by direct ink writing with kaolin suspensions. *J. Mater. Chem. C* **2018**, *6*, 11392.
(22) Francis, V.; Jain, P. K. Investigation on the Effect of Surface Modification of 3D Printed Parts by Nanoclay and Dimethyl Ketone. *Mater. Manuf. Process* **2018**, *33* (10), 1080−1092.
(23) Sajadi, S. M.; Boul, P. J.; Thaemlitz, C.; Meiyazhagan, A. K.; Puthirath, A. B.; Tiwary, C. S.; Rahman, M. M.; Ajayan, P. M. Direct Ink Writing of Cement Structures Modified with Nanoscale Additive. *Adv. Eng. Mater.* **2019**, *21* (8), 1801380.
(24) Pires, L. S. O.; Luís, J.; Fernandes, M. H. V.; Oliveira, M. Controlling properties of ceramic formulations for porcelain robocasting. *Ceram. Int.* **2023**, *49* (3), 4764−4774.
(25) Farahbakhsh, M.; Rybkowski, Z. K.; Zakira, U.; Kalantar, N.; Onifade, I. Impact of Robotic 3D Printing Process Parameters on Interlayer Bond Strength. *Autom. Constr.* **2022**, *142*, 104478.
(26) Pittayachaval, P.; Baothong, T. An Effect of Screw Extrusion Parameters on a Pottery Model Formed by a Clay Printing Machine. *Mater. Sci. Forum* **2021**, *1046*, 29−38.
(27) Fleck, T. J.; McCaw, J. C. S.; Son, S. F.; Gunduz, I. E.; Rhoads, J. F. Characterizing the Vibration-Assisted Printing of High Viscosity Clay Material. *Addit. Manuf.* **2021**, *47*, 102256.
(28) Marquez, C.; Mata, J. J.; Renteria, A.; Gonzalez, D.; Gomez, S. G.; Lopez, A.; Baca, A. N.; Nuñez, A.; Hassan, M. S.; Burke, V.; Perlasca, D.; Wang, Y.; Xiong, Y.; Kruichak, J. N.; Espalin, D.; Lin, Y. Direct Ink-Write Printing of Ceramic Clay with an Embedded Wireless Temperature and Relative Humidity Sensor. *Sensors* **2023**, *23* (6), 3352.
(29) Dzuy, N. Q.; Boger, D. V. Direct Yield Stress Measurement with the Vane Method. *J. Rheol.* **1985**, *29* (3), 335−347.
(30) Faksawat, K.; Limsuwan, P.; Naemchanthara, K. 3D printing technique of specific bone shape based on raw clay using hydroxyapatite as an additive material. *Appl. Clay Sci.* **2021**, *214*, 106269.
(31) Revelo, C. F.; Colorado, H. A. 3D printing of kaolinite clay ceramics using the Direct Ink Writing (DIW) technique. *Ceram. Int.* **2018**, *44* (5), 5673−5682.
(32) Ramachandran, V. S.; Lowery, M. S. Conduction Calorimetric Investigation of the Effect of Retarders on the Hydration of Portland Cement. *Thermochim. Acta* **1992**, *195*, 373−387.
(33) Rottstegge, J.; Wilhelm, M.; Spiess, H. W. Solid State NMR Investigations on the Role of Organic Admixtures on the Hydration of Cement Pastes. *Cem. Concr. Compos.* **2006**, *28* (5), 417−426.
(34) Liu, W.; Li, M.; Nie, J.; Wang, C.; Li, W.; Xing, Z. Synergy of Solid Loading and Printability of Ceramic Paste for Optimized Properties of Alumina via Stereolithography-Based 3D Printing. *J. Mater. Res. Technol.* **2020**, *9* (5), 11476−11483.
(35) Gu, Q.; Sun, L.; Ji, X.; Wang, H.; Yu, J.; Zhou, X. High-Performance and High-Precision Al_2O_3 Architectures Enabled by High-Solid-Loading, Graphene-Containing Slurries for Top-down DLP 3D Printing. *J. Eur. Ceram. Soc.* **2023**, *43* (1), 130−142.
(36) Lu, C.; Xu, Y.; Qi, D.; Qi, W.; Jiao, S.; Xiang, S. Preparation and Properties of 3D Printing Silica Ceramics. *Bull. Chin. Ceram. Soc.* **2018**, *37* (3), 939−943.
(37) Gu, Q.; Wang, H.; Gao, W.; Yu, J.; Zhou, X. Preparation of Large-Size Alumina Ceramic Parts by DLP 3D Printing Using High-Solid-Loading Paste and Optimizing the Debinding Process. *Ceram. Int.* **2023**, *49* (17,Part B), 28801−28812.
(38) Chan, S. S. L.; Pennings, R. M.; Edwards, L.; Franks, G. V. 3D Printing of Clay for Decorative Architectural Applications: Effect of Solids Volume Fraction on Rheology and Printability. *Addit. Manuf.* **2020**, *35*, 101335.
(39) Eqtesadi, S.; Motealleh, A.; Miranda, P.; Pajares, A.; Lemos, A.; Ferreira, J. M. F. Robocasting of 45S5 Bioactive Glass Scaffolds for Bone Tissue Engineering. *J. Eur. Ceram. Soc.* **2014**, *34* (1), 107−118.
(40) Smay, J. E.; Cesarano, J.; Lewis, J. A. Colloidal Inks for Directed Assembly of 3-D Periodic Structures. *Langmuir* **2002**, *18* (14), 5429−5437.

https://doi.org/10.1021/acsomega.4c02543
ACS Omega 2024, 9, 26450−26457

(41) Lejeune, M.; Chartier, T.; Dossou-Yovo, C.; Noguera, R. Ink-Jet Printing of Ceramic Micro-Pillar Arrays. *J. Eur. Ceram. Soc.* **2009**, *29* (5), 905−911.
(42) Yu, Y.; Zou, B.; Wang, X.; Huang, C. Rheological Behavior and Curing Deformation of Paste Containing 85 wt.% Al_2O_3 Ceramic during SLA-3D Printing. *Ceram. Int.* **2022**, *48* (17), 24560−24570.
(43) Liu, Y.; Huang, L.; Li, M.; Yan, P. The Effects of Sodium Citrate on Compressive Strength and Paste Microstructure of Self-Compacting Concrete. *Constr. Build. Mater.* **2020**, *260*, 120467.
(44) Mehrizi, S.; Sohi, M. H.; Saremi, M. Effect of Sodium Citrate as Complexing on Electrochemical Behavior and Speciation Diagrams of CoFeNiCu Baths. *Ionics* **2013**, *19* (6), 911−918.
(45) Liu, Y.; Zhang, Z.; Jing, R.; Yan, P. The Interaction of Sodium Citrate and Polycarboxylate-Based Superplasticizer on the Rheological Properties and Viscoelasticity of Cement-Based Materials. *Constr. Build. Mater.* **2021**, *293*, 123466.
(46) Li, Z. *Introduction to Engineering Geology*; China University of Geosciences Press: Hubei, 1994.
(47) Lamnini, S.; Elsayed, H.; Lakhdar, Y.; Baino, F.; Smeacetto, F.; Bernardo, E. Robocasting of Advanced Ceramics: Ink Optimization and Protocol to Predict the Printing Parameters - A Review. *Heliyon* **2022**, *8* (9), No. e10651.
(48) Zhang, C.; Luo, Z.; Liu, C.; Zhu, J.; Cao, J.; Yuan, J.; Wang, P.; Liu, C.; Lao, C.; Chen, Z. Dimensional Retention of Photocured Ceramic Units during 3D Printing and Sintering Processes. *Ceram. Int.* **2021**, *47* (8), 11097−11108.

https://doi.org/10.1021/acsomega.4c02543
ACS Omega 2024, 9, 26450−26457